

# A Flexure-Based Wrist for Needle-Sized Surgical Robots

Dylan P. Losey\*, Peter A. York\*, Philip J. Swaney, Jessica Burgner  
and Robert J. Webster III

Department of Mechanical Engineering, Vanderbilt University, Nashville, Tennessee, U.S.A.  
Vanderbilt Initiative in Surgery and Engineering, Nashville, Tennessee, U.S.A.

## ABSTRACT

We present a novel flexure-based wrist design intended for use with needle-sized robotic manipulators. It is designed to be mounted at the tip of a traditional surgical needle, deployed through an endoscope working channel, or attached to the tip of a concentric tube robot. In all these applications, the wrist enables dexterity in small spaces. The wrist consists of two stacked flexure joints that are actuated by thin pull wires. In this paper we present the design of the wrist, its kinematics, and an experimental evaluation of the relationship between actuation force and tip displacement conducted using a scale model.

**Keywords:** Miniature Wrist, Flexure, Continuum Robot, Robotic Surgery, Image-Guided Surgery, Image-Guided Therapy

## 1. INTRODUCTION

Needlescopic surgery (surgery done with tools less than 3 mm in diameter) holds great promise in reducing surgical invasiveness<sup>1</sup>. However, to accomplish needlescopic surgery with traditional straight, rigid tools, surgeons currently face all the same challenges they do in traditional laparoscopic surgery (lack of tool dexterity, poor ergonomics, etc.). Just as the wrists incorporated in the da Vinci surgical system<sup>2</sup> make it easier to use than traditional manual laparoscopic tools, wrists mounted to needlescopic manipulators can make them easier to use and thereby increase the complexity of the surgical procedures that can be attempted using them. Designing wrists at this size scale is challenging, and traditional pulley-based approaches like those used in the da Vinci system are infeasible.

Current trends in surgical robotics are also toward devices that are less invasive and more dexterous. Continuously flexible robots (known as “continuum robots”) are particularly useful in this context (see, for example <sup>3–6</sup> among many others) because of their ability to achieve controllable curved shapes. Concentric tube robots are a type of continuum robot that can be made with particularly small diameters, which are comparable to surgical needles. A concentric tube robot consists of a series of precurved, superelastic, concentric tubes that rotate and translate inside one another to create “tentacle-like” motion<sup>7,8</sup>. Surgical tools such as micro-forceps or a ring curette can then be attached to the tip of the innermost tube<sup>9</sup>.

These robots can be used in many areas of the human body as miniature manipulators and as steerable needles.<sup>10–15</sup> In contexts where they are used as miniature manipulators, both kinematic and anatomical constraints will partially restrict the movement of the cannula tip at the surgical site, particularly in terms of orientation. Thus a wrist mounted at the tip of the device has the potential to be useful to the surgeon, and further increase the dexterity of the overall system.

Thus, both needlescopic surgery and miniature robots motivate the development of small-scale surgical wrists. In view of this, prior designs have been developed based on ball joints<sup>16</sup>, universal joints<sup>17–19</sup>, and flexures<sup>4,20</sup>. A unique biologically-inspired wrist has even been proposed<sup>21</sup>. The vast majority of existing mechanisms are prototyped at diameters from 4–10 mm (see<sup>17</sup> for a review), though some recent designs have been proposed where it has been argued that they can be scaled down to 1.5–2.5 mm<sup>21,22</sup>. To increase the diversity of wrist design options available at this size scale, in this paper we propose a new flexure-based wrist mechanism. Primary design goals were simplicity of fabrication and construction, so we use only 2D profiles in flat sheets of material combined with thin wires. The wrist design we propose is scalable and has the potential to add three degrees of freedom at the tip of a concentric tube robot or needlescopic manipulator.

---

\*Shared First Authorship. Corresponding author: philip.j.swaney (at) vanderbilt.edu

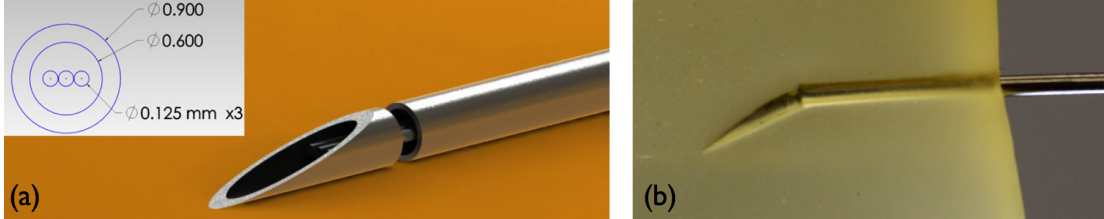


Figure 1. (a) Flexure tip needle design. The flexure is made from three 0.005" nitinol wires that lie along the centerline of the needle. (b) This allows the needle to bend in the direction of the bevel when inserted into tissue, while remaining stiff in the out of plane direction.

## 2. WRIST DESIGN

The inspiration for our flexure-based wrist design came from an idea to use a flexure as a passive joint between a needle shaft and beveled tip for use in needle steering<sup>23</sup>. Fixed “kinked tip” needles have been used in needle steering due to their increased radius of curvature over standard beveled tips<sup>24</sup>. However, when rapidly rotating a needle (“duty-cycling”) with a fixed kinked tip to achieve needle steering, tissue damage occurs as the tip cuts a helical track through tissue. The goal of the flexure tip needle was to create a needle tip design that could be straight when the needle was axially rotated, thus reducing the tissue damage, but act like a kinked tip to increase needle curvature if the needle was pushed through tissue without rotation. This necessitated a joint that required minimal force to flex, but would return to its straight configuration when axially rotated.

The flexure joint we created (see Figure 1) is made from three 0.005" diameter nitinol wires that lie along the centerline of the needle and can easily bend in the direction of the bevel upon insertion into tissue (see Figure 1b), while being stiff in the out-of-plane direction. The flexure joint met our objectives in needle steering experiments, and the prototype created demonstrated the feasibility of constructing a working flexure using thin nitinol wires inside a 0.9 mm diameter outer tube.

In this paper, we generalize this flexure mechanism, stacking two copies of it on top of one another while axially orienting them 90° apart, and attaching thin actuation wires to them to create a needle-sized wrist that can be robotically controlled. The wrist borrows the nitinol flexure joint from our steerable needle design and uses small discs to orient the nitinol wires appropriately. The discs (see Figure 2a) are designed to be cut with electrical discharge machining (EDM) out of a single piece of stainless steel. The nitinol wires that make up the flexure joint are located toward the periphery of the tube (see Figure 2b), leaving a central working channel for gripper actuation, suction, ablation, etc. The flexure joint wires are placed between the two discs to create a single flexure joint (see Figure 2b), and are glued in place using an adhesive. A second degree of freedom is achieved by placing an additional flexure joint on top of the first (see Figure 2c), and rotating it 90 degrees with respect to the bottom joint. Nitinol pull wires (tendons) that extend along the length of the wrist and loop back to the base of the wrist actuate the joints (see Figure 2d). Each degree of freedom uses two pull wires. The

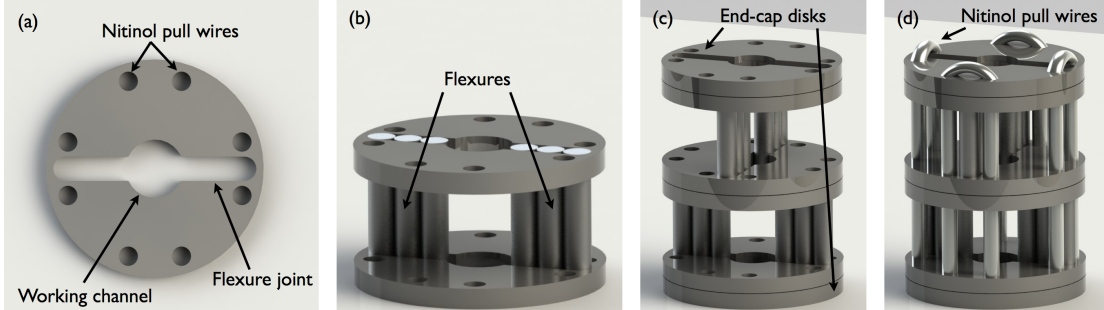


Figure 2. (a) Close-up of a CAD rendering of a single disc that aligns the nitinol wires that make up the flexure joint. (b) A single flexure joint, which is made of two discs that orient the nitinol wires. (c) Two flexure joints that are rotated 90° with respect to one another make up the wrist. (d) Pull wires are shown running along the length of the wrist. The wires are terminated at the tip of the wrist.

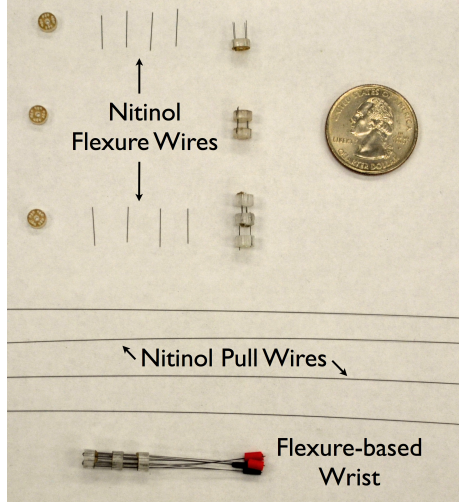


Figure 3. The different stages of the assembly process are shown here, along with a completed prototype wrist. Each wrist is comprised of eight nitinol flexure wires, four nitinol pull wires, and three acrylic discs. A quarter is shown to provide a sense of scale.

third degree of freedom comes from the ability to attach the wrist to an additional concentric tube just inside the innermost tube. This additional tube can be rotated, enabling the entire wrist to axially rotate.

## 2.1 Prototype Assembly

We fabricated several prototypes at a slightly larger scale than our design (dimensions larger by a ratio of  $\approx 3:1$ ) since these were straightforward to fabricate rapidly with the machining and manufacturing resources on hand, notably a KERN 150 W laser cutter (KER5225-150, USA) for cutting the discs. While the assembly of small scale mechanisms is typically challenging, the simplicity of our design made assembly straightforward. For our prototypes, the discs, including the holes through which the flexures and pull wires attach, were laser-cut from acrylic. The wrist prototype used for the displacement vs. position testing experiments described in Section 4 was made using 2.20 mm thick discs with diameter 5.0 mm. The wrist used for the force vs. displacement testing experiments was constructed from 2.80 mm thick discs with diameter 5.0 mm.

Nitinol wires with thickness 0.127 mm (0.005") were used for the flexures. We cut the wires to 10 mm in length, meaning that given disc thicknesses, the length of each flexure was 5.6 mm for the wrist with the 2.20 mm discs and 4.4 mm for the wrist with 2.80 mm discs. Four 10 mm long nitinol wires comprised a single flexure, with two wires on either side of the central channel. We note that changing the number of wires used to create a flexure, the diameter of the wires, and the placement of the wires will all change the performance of the wrist, creating a large design space for application specific wrist design. The pull wires were made from 0.150 mm (0.006") nitinol wires.

The assembly process is illustrated in Figure 3. One at a time, the ends of four nitinol wires, cut to 10 mm length, are dabbed in an adhesive (Loctite 406, Loctite, USA) and inserted with tweezers into the appropriate holes in one of the discs and allowed to dry. The opposite ends of all four wires are then dabbed in the adhesive, and another disc is inserted on top of the wet adhesive and allowed to dry. Next, another set of four nitinol wires cut to length are attached into another disc using adhesive and allowed to dry. We then attach the two pieces together with adhesive and run pull wires through to finish the assembly process. The final product is also shown in the figure, consisting of three discs, eight nitinol flexure wires, and four nitinol pull wires.

## 3. WRIST KINEMATICS

Here we model the miniature flexure wrist described above using Euler-Bernoulli beam theory. Treating the flexures as constant curvature continuum robots, we can apply a geometric argument and use the methods outlined in<sup>6</sup> to determine the forward kinematics as functions of both tendon (pull wire) tension and tendon

displacement. In order to derive our model we employ the following assumptions. As outlined in<sup>25</sup>, we assume that the bent and unbent flexures have the same curvature and dimensions for the purposes of calculating internal moments and forces and that the curvature of the flexures can be determined using linear constitutive relationships. We also assume that the cross-sectional position of the tendons within the discs does not vary, the tendons experience negligible friction and the tendons do not elongate. These are reasonable approximations, given that the proposed wrist design includes few discs, the tendon holes in the discs have a close tolerance with the tendons (their diameters differ by only 0.002"), and the wrist is actuated using nitinol tendons. We additionally make simplifying assumptions that the tendons cannot support internal moments or shear forces and that the out of plane flexures exhibit infinite stiffness. While the flexures are not infinitely stiff in the out of plane direction as assumed, it was shown that the out of plane stiffness is much greater than the in plane stiffness for a similar flexure design<sup>23</sup>. However, we do note that as the design is scaled down tendon stiffness may become important and out of plane stiffness may need to be explicitly modeled. We leave evaluation of these factors to future work, and proceed here with the above set of assumptions, which we experimentally illustrate later are good assumptions for the prototypes described and tested in this paper.

### 3.1 Wrist Model

We can simplify the backbone of our tendon-actuated continuum robot into a constant curvature continuum robot using the assumptions listed above and the miniature wrist geometry. The miniature wrist tendons and flexures are initially parallel and offset by a constant distance  $d$  (distance from the center of the disc to the tendon) as shown in Figure 4a and detailed in the above sections. When a tension  $f$  is applied to a tendon the flexures thus experience an instantaneous constant moment or pure bending (i.e. no shear force or shear stress). We assume that any change in flexure shape is negligible and thus the flexures always experience pure bending. This approximation is most accurate at low tensions (small displacements) and the accuracy will decrease as tension increases. These results may be extended to cases when adjacent tendons are actuated since our wrist is designed to decouple the flexure layers, and we have assumed that they are infinitely stiff in the out-of-plane direction. The curvature of a beam experiencing constant moment can be calculated using the Bernoulli-Euler beam equation

$$\kappa = \frac{M}{EI} = \frac{fd}{EI} \quad (1)$$

$E$  is the the Young's Modulus of the flexure and  $I$  is the cross-sectional moment of inertia. Since the applied moment ( $M$ ) is constant over the length of the flexure, the curvature  $\kappa$  of a flexure is also constant (1).

Following the notational framework outlined in<sup>6</sup>, given flexure curvature  $\kappa$ , we are able to find the homogeneous transformation, defined below as  $B(\phi_i)$ , for every point  $s$  along the arc  $[0, \ell]$ , where  $\phi$  is the plane rotation of the wrist. To obtain the final tip position of our wrist, we use several homogeneous transformations to go from the base of the wrist to the tip (see Figure 5). A prismatic transformation to account for the disc thickness

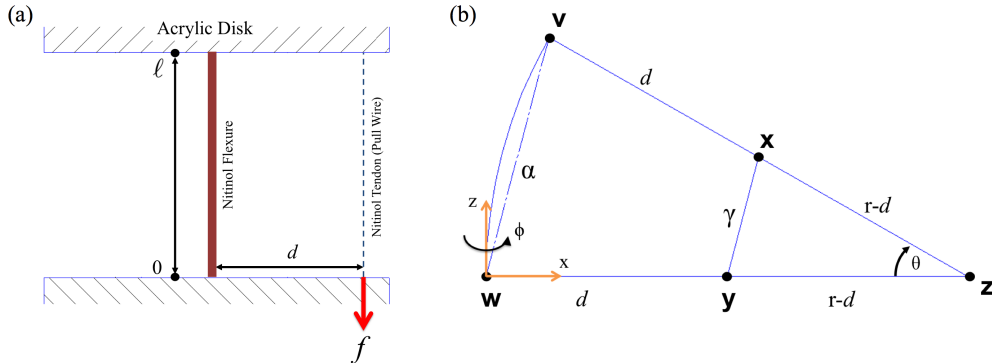


Figure 4. (a) A sketch showing some of the definitions used in the kinematics, including the derivation of the moment experienced by the flexure, which is  $fd$ . (b) Here, more geometric definitions are shown, including similar triangles  $\Delta vzw$  and  $\Delta xzy$ . The flexure top is defined as  $v$  and the flexure bottom is defined as  $w$ . Similarly,  $x$  is defined as the top of the tendon and  $y$  is the base of the tendon.

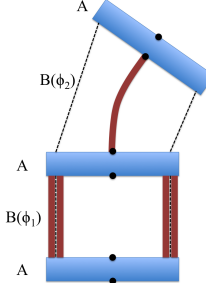


Figure 5. The homogeneous transformations used to determine the final wrist tip position are shown next to a drawing of the wrist.

is denoted as  $A$ , where  $t$  is the thickness of the disc, and the transformations along the flexures are denoted as  $B(\phi_i)$ . The complete transformation equation is given by

$$T_{tip} = AB_{\phi_1}AB_{\phi_2}A \quad (2)$$

where

$$A = \begin{bmatrix} 1 & 0 & 0 & 0 \\ 0 & 1 & 0 & 0 \\ 0 & 0 & 1 & t \\ 0 & 0 & 0 & 1 \end{bmatrix}, \quad B_{\phi_i} = \begin{bmatrix} \cos(\phi_i)\cos(\kappa s) & -\sin(\phi_i) & \cos(\phi_i)\sin(\kappa s) & \frac{\cos(\phi_i)(1-\cos(\kappa s))}{\kappa} \\ \sin(\phi_i)\cos(\kappa s) & \cos(\phi_i) & \sin(\phi_i)\sin(\kappa s) & \frac{\sin(\phi_i)(1-\cos(\kappa s))}{\kappa} \\ -\sin(\kappa s) & 0 & \cos(\kappa s) & \frac{\sin(\kappa s)}{\kappa} \\ 0 & 0 & 0 & 1 \end{bmatrix}. \quad (3)$$

In order to relate tendon displacement curvature ( $\kappa$  in (3)), we start with the equation for the displacement of the tendon, which is the length of the undeformed flexure ( $d$ ) minus the length of the actuating tendon path ( $\gamma$ ):

$$\delta = \ell - \gamma. \quad (4)$$

Referring to Figure 4, we can write an expression for  $\gamma$  by noting that  $\alpha$  and  $\gamma$  are the lengths of the corresponding sides of similar triangles. Thus  $\gamma$  can be written as,

$$\gamma = \alpha(1 - \kappa d). \quad (5)$$

The law of cosines defines  $\alpha$  as

$$(\alpha)^2 = \frac{2}{\kappa^2}(1 - \cos(\kappa s)). \quad (6)$$

We can disregard the negative solution for  $\alpha$  when taking the square root, since it corresponds to bending the flexure in the other direction (i.e. actuating the other tendon). Using (5) and (6) in (4), we arrive at an equation relating  $\delta$  and  $\kappa$ :

$$\delta = \ell - \sqrt{2}\left(\frac{1}{\kappa} - d\right)(1 - \cos(\kappa s))^{\frac{1}{2}}. \quad (7)$$

Since we can measure the input tendon displacement, we can solve (7) for curvature using MATLAB's `fsolve` function. We then use the resulting curvature to define the position of any point along the wrist backbone using (2). If, on the other hand, we choose to measure tendon tension ( $f$ ) rather than displacement, we can still solve for  $\kappa$  using (1). In summary, we have shown in this section how to use classical beam mechanics model our flexure-based wrist, describing its tip position in terms of either tendon tension or tendon displacement.

#### 4. EXPERIMENTAL RESULTS

In order to test our model, we performed two experiments. In the first, we measured the tip position of the wrist given a known displacement of the tendon, and in the second we measured the tip position of the wrist given a known tension applied to the tendon. The base frame of the kinematic model was aligned with the physical base frame of the wrist by deflecting the wrist, collecting data, and fitting a plane to the data to obtain the plane of bending. The rotation within that plane was adjusted such that both curves were tangent at the origin.

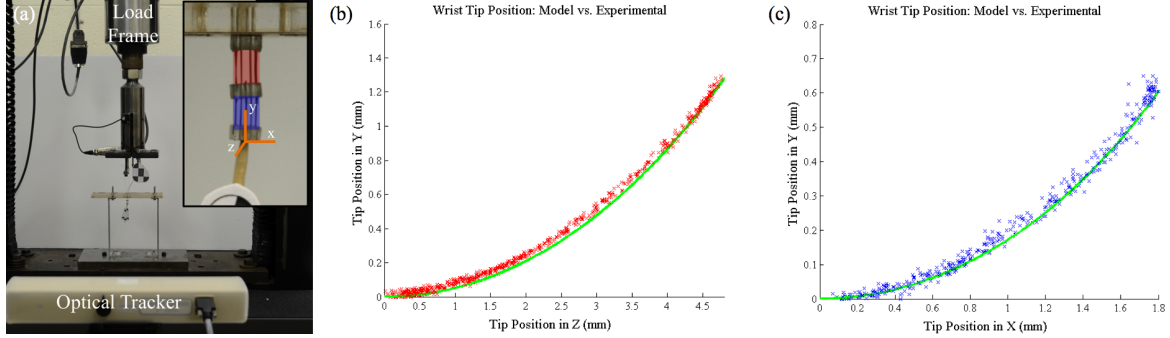


Figure 6. (a) The setup used to measure tendon displacement vs. tip position is shown. The load frame displaced a single tendon, while an optical tracker measured the displacement of the tip of the wrist. These results were then compared against the kinematic displacement model developed in Section 3. The shaded color of the wrist corresponds to the experimental data shown in plots (b) and (c), while the model prediction is always shown in green.

#### 4.1 Tendon Displacement vs. Tip Position

For this experiment, we used a load frame (Instru-Met Total Frame, USA) that displaced the tendon. We optically tracked the tip of the wrist and the displacement of the tendon using a Micron Tracker (Claron Technology, Ontario, Canada). The tracker recorded a stream of data at 16 Hz during the displacement of the tendon. The experimental setup used is shown in Figure 6a. Our experimental results are overlaid on our model prediction in Figures 6b and 6c. Note that the color of the experimental data corresponds to the flexure joint that was actuated, as seen in Figure 6a. The model prediction is shown in green. It can be seen that the model fits the data very well, and only begins to deviate at high curvature values, which may be due to out of plane bending caused by misalignment of the flexures during assembly as well as buckling of the nitinol flexures. An error comparison of the model predicted position to the experimental data is shown in Table 1.

Table 1. Tendon Displacement vs. Tip Position Error

	Red Flexure			Blue Flexure		
	X	Y	Z	X	Y	Z
Mean (mm)	0.035	0.438	0.100	0.073	0.020	0.099
Std. Dev. (mm)	0.027	0.234	0.093	0.049	0.017	0.076

#### 4.2 Tendon Tension vs. Tip Position

To obtain the tension in the tendon, we hung known weights from the tendon and recorded the tip position for each weight. We incremented the weight by 5 g from 0 g to 100 g. The experimental setup used in this experiment

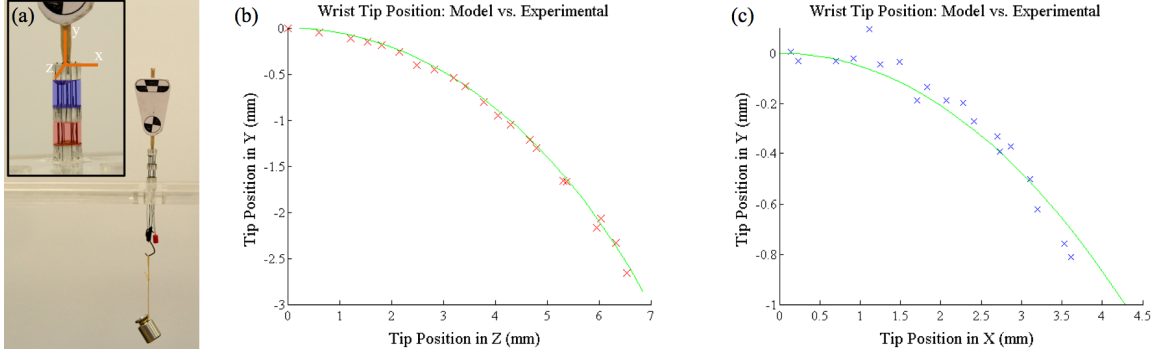


Figure 7. Weights were hung from a single tendon in increments of 5 g to 100 g while the tip of the wrist was measured using the optical tracker. The experimental data is compared against the kinematic force model in plots (b) and (c).

is shown in Figure 7a, and the experimental data overlaid on the model prediction is shown in Figures 7b and 7c. An error comparison of the model predicted position to the experimental data is shown in Table 2.

Table 2. Tendon Tension vs. Tip Position Error

	Red Flexure			Blue Flexure		
	X	Y	Z	X	Y	Z
Mean (mm)	0.089	0.198	0.069	0.390	0.126	0.110
Std. Dev. (mm)	0.073	0.139	0.054	0.179	0.083	0.106

## 5. DISCUSSION AND CONCLUSIONS

This paper presents early steps toward developing a new flexure-based wrist design for needle sized manipulators. We constructed and performed experiments on a scale model of the wrist at approximately 3:1 scale and developed a simple kinematic model which was tested against the prototype wrist. It appears that this design will be useful for enhancing dexterity in these devices, and will provide another design option for engineers seeking to construct wrists at this size scale. One can get an idea of the workspace of our first prototypes from Figure 8. There are several improvements that will be made as the work progresses, particularly with the manufacturing and assembly process, as we believe misalignments of the flexure wires and imprecise spacing of the disks led to out of plane bending of the wrist. The manufacturing process could be improved through the use of fixtures to allow for more repeatable and accurate assembly. We will wire EDM the disks for the next prototype at true scale, or 1.5 mm in diameter.

In addition to improvements in manufacturing and assembly of the wrist, we will continue to improve and refine our model. We would like to improve the kinematic precision of our model by means of the Cosserat rod and extensible strings models. Our ongoing work includes applying the method proposed in<sup>25</sup> to our unique wrist design. In this paper, we did not consider any coupling between the flexure links nor buckling of the flexure, although we know coupling does exist and the nitinol flexures can buckle, and we intend to include these effects in future models. We will also begin looking at the large design space available with this wrist, notably the length and diameter of the flexure wires, as well as the geometry of the disks. This will enable us to optimize the wrist for various surgical procedures.

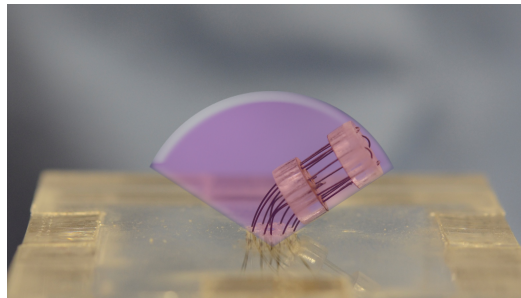


Figure 8. The purple overlay is the workspace of our flexure based wrist, assuming that the wrist is mounted to a tube that may be rotated, such as our concentric tube robot.

## ACKNOWLEDGMENTS

This work was supported in part by a National Science Foundation (NSF) Graduate Fellowship and in part by NSF grant IIS-1054331. Any opinions, findings, and conclusions or recommendations expressed in this material are those of the author(s) and do not necessarily reflect the views of the NSF.

## REFERENCES

- [1] Mamazza, J., Schlachta, C. M., Seshadri, P. A., Cadeddu, M. O., and Poulin, E. C., "Needlescopic surgery. A logical evolution from conventional laparoscopic surgery," *Surgical endoscopy* **15**(10), 1208–12 (2001).
- [2] Guthart, G. S. and Salisbury, J. K., "The Intuitive<sup>TM</sup> telesurgery system: Overview and application," in *International Conference on Robotics and Automation*, 618–621 (2000).
- [3] Dario, P., Paggetti, C., Troisfontaine, N., Papa, E., Ciucci, T., Carrozza, M. C., and Marcacci, M., "A Miniature Steerable End-Effector for Application in an Integrated System for Computer-Assisted Arthroscopy," in *International Conference on Robotics and Automation*, 1573–1579 (1997).
- [4] Peirs, J., Reynaerts, D., Van Brussel, H., and De Gersem, G., "Design of an Advanced Tool Guiding System for Robotic Surgery," in *International Conference on Robotics and Automation*, 2651–2656 (2003).
- [5] Simaan, N., Xu, K., Wei, W., Kapoor, A., Kazanzides, P., Taylor, R., and Flint, P., "Design and Integration of a Telerobotic System for Minimally Invasive Surgery of the Throat," *The International Journal of Robotics Research* **28**(9), 1134–1153 (2009).
- [6] Webster III, R. J. and Jones, B. A., "Design and kinematic modeling of constant curvature continuum robots: A review," *International Journal of Robotics Research* **29**(13), 1661–1683 (2010).
- [7] Rucker, D. C., Webster III, R. J., Chirikjian, G. S., and Cowan, N. J., "Equilibrium Conformations of Concentric-tube Continuum Robots," *The International Journal of Robotics Research* **29**(10), 1263–1280 (2010).
- [8] Dupont, P. E., Lock, J., Itkowitz, B., and Butler, E., "Design and Control of Concentric-Tube Robots," *Transaction on Robotics* **26**(2), 209–225 (2010).
- [9] Gilbert, H. B., Swaney, P. J., Burgner, J., Weaver, K. D., Russell III, P. T., and Webster III, R. J., "A feasibility study on the use of concentric tube continuum robots for endonasal skull base tumor removal," *Hamlyn Symposium on Medical Robotics* (2012).
- [10] Swaney, P. J., Burgner, J., Pheiffer, T. S., Rucker, D. C., Gilbert, H. B., Ondrake, J. E., Simpson, A. L., Burdette, E. C., Miga, M. I., and Webster III, R. J., "Tracked 3D ultrasound targeting with an active cannula," *SPIE Medical Imaging* (2012).
- [11] Comber, D. B., Cardona, D., Webster III, R. J., and Barth, E. J., "Precision pneumatic robot for MRI-guided neurosurgery," *Design of Medical Devices Conference* (2012).
- [12] Lyons, L. A., Webster III, R. J., and Alterovitz, R., "Planning active cannula configurations through tubular anatomy," in *International Conference on Robotics and Automation*, 2082–2087 (2010).
- [13] Gosline, A. H., Vasilyev, N. V., Butler, E. J., Folk, C., Cohen, A., Chen, R., Lang, N., del Nido, P. J., and Dupont, P. E., "Percutaneous intracardiac beating-heart surgery using metal mems tissue approximation tools," *The International Journal of Robotics Research* **31**(9), 1081–1093 (2012).
- [14] Anor, T., Madsen, J. R., and Dupont, P. E., "Algorithms for Design of Continuum Robots Using the Concentric Tubes Approach: A Neurosurgical Example," in *International Conference on Robotics and Automation*, 667–673 (2011).
- [15] Burgner, J., Swaney, P. J., Rucker, D. C., Gilbert, H. B., Nill, S. T., Russell, P. T., Weaver, K. D., and Webster III, R. J., "A bimanual teleoperated system for endonasal skull base surgery," in *International Conference on Intelligent Robots and Systems*, 2517–2523 (2011).
- [16] Harada, K., Tsubouchi, K., Fujie, M., and Chiba, T., "Micro manipulators for intrauterine fetal surgery in an open mri," in *International Conference on Robotics and Automation*, 502–507 (2005).
- [17] Van Meer, F., Giraud, A., Esteve, D., and Dollat, X., "A disposable plastic compact wrist for smart minimally invasive surgical tools," in *International Conference on Intelligent Robots and Systems*, 919–924 (2005).
- [18] Shang, J., Noonan, D., Payne, C., Clark, J., Sodergren, M., Darzi, A., and Yang, G.-Z., "An articulated universal joint based flexible access robot for minimally invasive surgery," in *International Conference on Robotics and Automation*, 1147–1152 (2011).
- [19] Ishii, C. and Kobayashi, K., "Development of a new bending mechanism and its application to robotic forceps manipulator," in *International Conference on Robotics and Automation*, 238–243 (2007).

- [20] Arata, J., Saito, Y., and Fujimoto, H., "Outer shell type 2 DOF bending manipulator using spring-link mechanism for medical applications," in *International Conference on Robotics and Automation*, 1041–1046 (2010).
- [21] Breedveld, P., Sheltens, J., Blom, E., and Verheij, J., "A new, easily miniaturized steerable endoscope," *Engineering in Medicine and Biology Magazine* **24**(6), 40–47 (2005).
- [22] Sieklicki, W., Zoppi, M., and Molfino, R., "Superelastic compliant mechanisms for needlescopic surgical wrists," in *International Conference on Reconfigurable Mechanisms and Robots*, 392–399 (2009).
- [23] Swaney, P. J., Burgner, J., Gilbert, H. B., and Webster III, R. J., "A Flexure-Based Steerable Needle: High Curvature with Reduced Tissue Damage," *Transactions on Biomedical Engineering* (2013). In Press.
- [24] Wedlick, T. R. and Okamura, A. M., "Characterization of Pre-Curved Needles for Steering in Tissue," in *International Conference of the IEEE Engineering in Medicine and Biology Society*, 1200–1203 (2009).
- [25] Rucker, D. C. and Webster III, R. J., "Statics and dynamics of continuum robots with general tendon routing and external loading," *Transactions on Robotics* **27**(6), 1033–1044 (2011).